The PI-methods for Helical Cone-Beam Tomography

Per-Erik Danielsson, Maria Magnusson Seger, and Henrik Turbell[1)]
Dept of EE, Linköping University, IVP Integrated Vision Products[1)]
SE-581 83 Linköping, Sweden, SE-583 30 Linköping, Sweden[1)]

Abstract. Next generation helical cone-beam CT will feature pitches around 80 mm. It is predicted that reconstruction algorithms to be used in these machines with still rather modest cone angles may not necessarily be exact, but rather have an emphasis on simplicity and speed. The PI-methods are a family of algorithms, all of which are based on complete data capture with a detector collimated to the Tam-window followed by rebinning to obliquely parallel ray geometry. The non-exactness is identified as inconsistency in the space invariant one-dimensional ramp-filtering step. It is shown that this inconsistency can be reduced resulting in significant improvement in image quality and increased tolerance for higher pitch and cone angle.

1. Introduction

Three-dimensional reconstruction algorithms in general are conveniently divided into exact[1] and non-exact algorithms. The first exact algorithms for helical cone-beam scanning (Tam 1995) were straight-forward extensions of Grangeat's result (Grangeat 1987), which required that the totality of available projections covered the object in full. However, a practical requirement for any new method is the ability to cope with the long object problem (Danielsson *et al* 1997). A recent evaluation of three exact algorithms for this purpose has been presented (Sourbelle *et al* 2001). Even more recent are the methods by Katsevich (2001), Kudo et al (2001) and Hu et al (2001). However, as pointed out by Defrise et al (2001), the numerical complexity of the exact algorithms tends to increase the execution time and call for extra precautions to combat discretization errors and loss of resolution.

The next generation of CT-machines will have moderately high pitches around 80 mm, which means cone angles less than ± 2 degrees. Even so, the speed will be impressive. With a gantry that rotates 2.5 r/sec a body section of 20 cm is covered in 2 seconds. Therefore, in the wake of potential implementation problems for the exact methods, non-exact algorithms with inherent simplicity are of considerable interest. The number of such non-exact (approximate) algorithms is steadily increasing (Turbell et al 2000). Among more recent proposals are the one by Strierhofer et al (2001) where a slice is composed by segmented planes, each one being narrow enough to allow for 2D-reconstruction.

The PI-detector fits exactly the Tam window (Tam 1995), the area between two consecutive turns of the helix. Figure 1 illustrates the ray geometry for this detector in its rebinned and non-rebinned versions. As we show in the next section, the data capture is complete and (almost) non-redundant (Danielsson et al 1997). This is the reason why all exact and an increasing number of non-exact methods are using the PI-detector.

[1] A reconstruction algorithm is *exact* if any requirement on fidelity to the original can be met, provided that accurate and noise-free projection are data captured with sufficient density along a source trajectory, which meets some specific conditions for completeness.

2. The PI-line

A PI-line is defined to be any line that has two points on the helix less than 360 degrees apart (Danielsson et al 1997). Accordingly, a *PI-segment* is the segment of a PI-line inside the helix. The PI-reconstruction methods to be described in the next sections are based on the following three observations of the PI-segments.

Observation 1). As the object cylinder rotates upwards in the fixed source-detector system in Figure 1a), at the first instant of exposure the PI-segment is a ray-path projecting its content onto a point at the upper edge of the detector. After a 180-degree rotation as seen from a point on the PI-segment itself, this PI-segment becomes a perfect ray-path for the second time. Again a ray projects its content onto a single detector point although at the lower edge of the detector. Hence, all PI-segments are projected over 180 degrees as seen from themselves.

Observation 2). We study the local Fourier transform of a small sub-volume on a PI-line in the manner of Orlov (1975). The distance to the source is so large that the divergence of the cone-beam is negligible and we may assume that the volume is projected by a parallel beam. The 180-degree exposure can then be portrayed as in Figure 2. The point-shaped object is in the center of a unit sphere. A source path is laid out on this sphere from the entrance angle A to the diametrically opposite exit angle B. We should also imagine that the 3D Fourier transform of the small object is overlaid this space and centered at the origin.

The arbitrary frequency component D is normal to a central plane, which is sectioning the Fourier space as well as the unit sphere onto which we have mapped the source trajectory. By virtue of the Fourier slice theorem, a source position on this plane will generate projections, which contains the frequency component D. The source trajectory from A to B has to cross this plane, say, at C, so that the projection taken from this source position will include D. Therefore, each Fourier component of each small sub-volume on a PI-line is included in the projection data. If A and B are not diametrically opposite there would be room for a central Fourier plane not crossed by the source path. The 180-degree exposure guarantees complete data capture.

Observation 3). Figure 3 will help us to see that every point inside the helix cylinder is on a PI-line. Select an arbitrary point A. The horizontal plane through A (indicated by a horizontal circle through the helix cylinder) will intersect the helix at B. Let the line BAC rotate around A, while B keeps contact with the helix sliding upwards. During this process, let the other end C keep its contact with the helix *cylinder* surface. Both C and B are leaving the horizontal plane, but while we force B to move along the helix left- and upwards towards B', C is moving right- and downwards towards C'. This point on the helix is reached before the line has rotated 180 degrees. The original horizontal line has now become the PI-line B'AC' to which A belongs. Also, point A cannot belong to any other PI-line. A futile attempt would be to find a second PI-segment as AC'' in Figure 3 but in order to land with the other end B'' of the line segment on the helix, we have to slide and rotate AC'' to the right until it coincides with B'AC'. Hence, each object point belongs to one and only one PI-segment.

The above three observations and conclusions can be summarized in the conjecture that *the PI-detector is performing a complete data capture of the object space*. This is consistent with the fact that the same data capture has proven to be

sufficient and necessary for exact reconstruction (Tam 1995). However, the conjecture also indicates that as soon as the data capture for a small sub-volume is complete it should be possible to reconstruct this sub-volume. In so doing, the long object problem would also be solved. Interestingly, the most recently invented exact method by Katsevic (2001) is indeed able execute its reconstruction without involving projection data from far-away parts of the long object. The same feature also holds for the PI-methods to be presented here.

3. PI-ORIGINAL

In the rebinned geometry Fig. 1b), a set of obliquely parallel PI-segments will enter and exit the illuminated area simultaneously. These PI-segments and their object points are residing on a continuous non-planar surface, which we call a *PI-surface*. As a consequence to the above observation 3), the set of successive PI-surfaces are non-overlapping but nutated with respect to each other, while completely filling the object space.

The discovery of the *original PI-method* (Danielsson et al 1998) was based on the simple insight that the above rebinned ray geometry guarantees that the backprojection step will deliver the same number of contributions to all object points. No special consideration except simplicity was given to the filtering step.The PI-ORIGINAL algorithm consists of the following four steps.

1) *Pre-weighting* of detector data with cosine of the cone angle
2) *Rebinning* to obliquely parallel projection data on the virtual detector
3) *Rampfiltering* of rebinned data row-by-row
4) *Backprojection* along the original ray paths without magnification factor

Considering the extreme simplicity of the algorithm, we found the results encouraging (see below under 6. Experiments) and a stimulus for further research and improvements. One such development became the *n-PI methods* reported by Proksa et al (2000), where n is any odd number. The original PI-method is the 1-PI method. The 3-PI method utilizes a detector bounded by three consecutive turns; the 5-PI method has a detector bounded by five consecutive turns, etc. It can then be shown (although less trivially than expected) that each object point is indeed exposed during a rotation interval of $n\pi$. In practice, this family of methods can use (almost) the same physical detector. For the n-PI case, the patient is just translated n times slower than for 1-PI, all other parameters being constant. The pitch and the cone angle become proportional to $1/n$. With constant photon flux from the source the expected signal-to-noise ratio is proportional to $\sqrt{n}$. The family of n-PI-methods taken together forms a powerful system able to utilize much higher cone angles than $\pm 2^0$ by trading speed for artifact and noise reduction.

4. PI-SLANT and PI-2D

Definition. A reconstruction using filtered back-projection is *consistent* if the object points to be reconstructed are divided into sets so that all points within a set participate in all projection events (all projection angles), as well as in all filtering events and all back-projection events.

Ordinary planar slice-by-slice two-dimensional reconstruction is fully consistent. A typical inconsistency occurs when truly 3D-reconstruction is approximated with 2D-

versions. Although we have not (yet) defined a measure of inconsistency, we take it for granted that such a measure can be defined and we allow ourselves to talk about degrees of consistency, minimizing inconsistency and so on. We also take it for granted that there is a strong correlation between inconsistency and non-exactness in the reconstruction. To minimize inconsistency in the original PI-method, we try to localize disjunctive 2D sets of object points which are nearly possible to project with a 1D-set of rays throughout the 180 degree rotation. Natural candidates for such sets are the PI-surfaces. The PI-surface is not perfectly planar but slightly saddle-shaped. During the rotation the projection of the points of a PI-surface will be centered along a slanted line, which is the projection of the mid-ray in the PI-surface.

In Figure 4 we see the projections of the points of a PI-surface for nine rotation positions in the interval from $\theta = 0^0$ to $\theta = 180^0$. For the top and bottom rows the ramp-filtering along horizontal rows as in PI-ORIGINAL is correct (consistent) with respect to the PI-surfaces. But for the better part of the exposure interval it is highly inconsistent. In the five-step **PI-SLANT** algorithm below, the filtering instead takes place along the slanted mid-lines of the projections.

1) *Pre-weighting* of detector data with cosine of the cone angle
2) *Rebinning* (horizontally) to obliquely parallel projection data
3) *Resampling* (vertically) to sets of slanted lines
4) *Ramp-filtering* along slanted lines
5) *Backprojection* along the original ray paths without magnification factor

Filtering of this kind aiming for maximum consistency was proposed by Larson et al (1998) and Heuscher (1999). However, the filtered data were then back-projected into the 2D-surface instead of into the 3D-volume as in PI-SLANT. This results in inconsistency between the actual ray-paths for projection and back-projection. To find out if such a strategy is viable we designed a variation of PI-SLANT we call PI-2D. Here, the back-projection in the last step means back-projection into the two-dimensional PI-surface even if the original projection rays are far from perfectly embedded in the PI-surface. From the reconstruction experiments to be shown below, we draw the conclusion that 3D back-projection along the original rays as in PI-SLANT is a superior technique. Unfortunately, 3PI- and other *n*-PI-methods are not applicable to slanted ramp-filtering.

5. PI-FAST

Although the ramp-filtering inconsistency is significantly reduced in PI-SLANT compared to PI-ORIGINAL it is not reduced to zero. Full consistency would require two-dimensional filtering, but further reduction of inconsistency might still be possible with 1D ramp-filtering. The projection data collected by the virtual PI-detector form a 3D-data set $p(\theta, s, t)$, a kind of 3D-sinogram. Each object point delivers contributions to $p(\theta, s, t)$ along a 3D-curve, which projected onto the (θ, t)-plane is a perfect sinusoid. For each object point in the reconstructed volume the back-projection we are employing is faithfully accumulating the filtered projection data along the same individual 3D-curves.

Figure 4 is a projection of $p(\theta, s, t)$ along the θ-axis, which illustrates how the projection of the non-planar PI-surface tilts and bends as it moves from entrance to exit. The points of the PI-surface are dispersed in the vertical direction, mostly so for $\theta = 45^0$ and 135^0. The dispersion makes the ramp-filter exchange signal energy between

object points in different PI-surfaces, a sign of remaining inconsistency in PI-SLANT. In the PI-FAST-algorithm we attempt to diminish this interaction by letting the ramp-filtering as well as the Back-Projection (BP) operate in the 3D-projection space $p(\theta, s, t)$.

Fast back-projection is a technique, which is simple to understand in the 2D-case, (see for instance Brandt et al 1999). Rather than injecting tiny contributions into all voxels for each projection (detector-driven BP), or summing along the full length of one sinusoid at a time (voxel-driven BP), fast back-projection accumulates limited sets of projection data in the sinogram along short sinusoid segments. These short segments are called *links*. In the next step we sum these link values (with interpolation) into longer links etc, until we have obtained the sums along all full-length sinusoids of interest, which means the image is done. It can be shown that the complexity of $O(N^3)$ for traditional back-projection can be reduced to $O(N^2 \log N)$ with fast back-projection, which renders this method the epithet fast.

Figure 5 shows how fast back-projection makes it possible to postpone the ramp-filtering in 2D FB. In Fig.5a) the circles indicate projection data in the sinogram. The slanted lines indicate seven links of length five. Traditional ramp-filtering with a convolution kernel $g(t)$ followed by back-projection takes place with the upper formula for link-computation in Figure 5. However, as long as the links are parallel this computation is identical to the formula below where we sum (back-project) first and ramp-filter afterwards. In the 2D-case, there is no point in doing this. The complete set of links in Fig.5b) are all in plane and all projection data should interact with each other in this manner anyway. In the 3D-case, however, the corresponding link structure is three-dimensional. Two different sets of parallel links such as in Figure 5b) might not be in-plane but slightly oblique to each other as they follow the slopes of different PI-surfaces.

The 3D-link structure for a PI-surface is embedded in the (θ, s, t)-space and can be precompiled in detail (Turbell 2001). At entrance and exit (top and bottom of Figure 4) the 3D-structure of a PI-surface is thinned down to sheet, while it has a certain thickness in between. This is where PI-FAST makes a difference and the two formulas in Figure 5 take on different values. This algorithm consists of the following six procedures. The links to be used in PI-FAST are of intermediate length covering a limited portion of the θ-interval of π radians.

1) *Pre-weighting* of detector data with the cosine of the cone angle
2) *Rebinning* to obliquely parallel projection data on the virtual detector
For all PI-surfaces
   3) *Back-projection 1*: Accumulating link values over (typically) 16 angles
   4) *Ramp-filtering* the sets of link values
   5) *Backprojection 2:* Accumulating the final pixel values
6) *Resampling* the pixel values of the PI-surfaces in the z-direction to the Cartesian grid.

6. Experiments

We conducted six experiments with parameters for geometry, reconstruction, and presentation given by the following table. The detector element size (1.56 *mm*, also used for the reconstruction grid) is measured on the virtual detector at rotation center (2.4 *mm* on the physical detector). This resolution is only half of what is customary but sufficient

for comparison of artifacts. In Experiment 1, presented in Figures 6 and 7, we apply the above four PI-methods to the Clock and the Shepp-Logan phantoms, respectively. The Clock phantom has some features common with a human body, while the well-known 3D Shepp-Logan phantom bears some similarity to a human head with interior low contrast features. The clock phantom consists of an object cylinder with 0 *HU* on a background of -1000 *HU*. Inside are two sets of spheres with 400 *HU* arranged in a clockwise fashion and gradually offset in the z-direction. For image quality evaluation in Figure 6 we also show the same slice (thickness 1.56*mm*) reconstructed with the "golden standard" 2D FB, as well as a PI-ORIGINAL slice reconstructed in full resolution (Exp. 0) and slice thickness 0.79*mm*. In Experiments 2 - 5, presented in Figure 8, we employ the Clock phantom only. The purpose is to demonstrate the sensitivity to higher fan and cone beams.

	Exp. 0	*Exp 1*	*Exp.2*	*Exp.3*	*Exp.4*	*Exp.5*
Helix radius *R*	570 *mm*	570 *mm*	760 *mm*	400 *mm*	760*mm*	400 *mm*
Pitch *P*	81.25 *mm*	81.25 *mm*	187.5 *mm*	100 *mm*	381.25 *mm*	200 *mm*
Field of view	400 *mm*	400 *mm*	400 *mm*	400 *mm*	400 *mm*	400 *mm*
Fan angle	± 20.54	± 20.54	$\pm 15.26^0$	$\pm 30^0$	$\pm 15.26^0$	$\pm 30^0$
Cone angle	$\pm 2.04^0$	$\pm 2.04^0$	$\pm 3.51^0$	$\pm 3.58^0$	$\pm 7.15^0$	$\pm 7.13^0$
# views per turn	1024	512	512	512	512	512
# detector rows	52	26	60	32	122	64
# elem. per row	511	255	255	255	255	255
Element size	$0.78^2\ mm^2$	$1.56^2\ mm^2$	$1.56^2\ mm^2$	$1.56^2\ mm^2$	$1.56^2\ mm^2$	$1.56^2\ mm^2$
Voxel size	$0.78^3\ mm^3$	$1.56^3\ mm^3$	$1.56^3\ mm^3$	$1.56^3\ mm^3$	$1.56^3\ mm^3$	$1.56^3\ mm^3$
Slice thickness	0.78 *mm*	1.56 *mm*	1.56 *mm*	1.56 *mm*	1.56 *mm*	1.56 *mm*
Reconstr. grid	512x512	256x256	256x256	256x256	256x256	256x256

7. Discussion and Conclusions

See Fig. 6. Clearly, we can never expect to get better image quality than the 2D reconstructed result from parallel projections shown in the upper left. PI-original contains some steak artifacts and some shadows below some spheres. Still, the image quality is vastly better than PI-2D. We attribute the special type of strong "skewing" artifacts in the PI-2D to the inconsistent back-projection geometry. PI-SLANT, and even more so PI-FAST, have less shadow and streak artefacts than PI-ORIGINAL.

Full grid and detector resolution was applied in the PI-ORIGINAL-reconstruction in Exp. 0. with the result at top right in Fig. 6. The full detector resolution at the virtual detector is $0.78^2\ mm^2$, which increases to $1.2^2\ mm^2$ on a physical source-centered detector array at the distance 870 *mm.*

The size of the cross-cut disks in Figure 6 seems to match the golden standard for all methods except in two cases. The large sphere at 10 o'clock and the small sphere at 5 o'clock are sliced just at the top and in these cases the disks become enlarged in most of the 3D-reconstructed images. The reason is that all 3D-methods involve vertical interpolation on the detector, which creates extra smoothing of edges. In he full resolution PI-ORIGINAL the smoothing/enlargement is proportionally smaller. This seems to be the most significant difference between the two images at top center and right in Fig. 6.

All methods are doing remarkably well for the Shepp-Logan phantom in Figure 7, in spite of the narrow gray-level window of $\pm 20\,HU$. From a glance at the more artifact-ridden images to follow in Figure 8, we conclude that the Shepp-Logan phantom is just too easy.

The geometry in the experiments 2, 3, 4, and 5 (Figure 8) are chosen to find out how gracefully the four PI-methods are degrading for increased cone and fan angles. Clearly the image quality ranking from worse to best is here PI-2D, PI-ORIGINAL, PI-SLANT and PI-FAST. The PI-2D-method is doing quite badly for these more demanding geometries. PI-ORIGINAL suffers from shadow artifacts. Some shadows are also visible in PI-SLANT and PI-FAST, although to a much lesser extent. The two upper rows (same cone angle, different fan angles) are almost identical and so are the two lower ones. We conclude that the quality hinges primarily on the cone-beam angle and to a much lesser extent on the fan angle. This is far from evident, since the PI-surfaces are quite planar for small fan angles, which could be expected to pay off in less artifacts for non-exact methods.

For which cone angle ranges are then these methods practically useful? Clearly, precise image quality measures and much more exhaustive experiments are required to answer this question. However, we believe that the strong artifacts for PI-2D in Figure 6 (cone angle $\pm 2^0$ only) makes these methods less uninteresting. We believe this forecast also holds for related methods using nutated surfaces or planes such as (Heuscher 1999) and (Larson et al 1998) as well as for all SSRB-techniques (Noo et al 1998). Inconsistency between projection and back-projection geometry is not recommendable. PI-ORIGINAL should give better images and is probably simpler to implement than these 2D-back-projection methods. PI-SLANT is not quite as simple but delivers somewhat better images. Hence, this method should be practically useful well beyond the cone angle range of $\pm 2^0$, at least for fast scanning and medium image quality imaging. The PI-FAST holds out even better for the rather extreme geometries in Figure 8. Unfortunately, this method issignificantly more complicated than the other PI-methods and, in spite of its name, it is also slower.

Acknowledgement This work was supported by Philips Medical Research, Hamburg, Germany, which is hereby gratefully acknowledged.

References

Brandt, A., Mann, J., Brodski, M., Galun, M. (1999), A fast and accurate multilevel inversion of the Radon transform. *SIAM Journal of Applied Mathematics*, **60** 437-462.

Danielsson P.-E., Edholm P., Eriksson J., and Magnusson-Seger M., (1997) Towards Exact 3D-reconstruction for Helical Cone-Beam Scanning of Long Objects: A New Arrangement and a New Completeness Condition, *3D-1997, The fourth int. meeting on fully three-dimensional image reconstruction in radiology and nuclear medicine*, Nemacolin, PA, USA, pp. 141-144, June 25-28

Danielsson, P.-E., Edholm, P., Eriksson, J., Magnusson-Seger, M., and Turbell, H, (1998), Helical cone-beam scanning an reconstruction of long objects using 180 degree exposure, Patent Appl. PCT/SE 98/00029, Filed Jan.13, 1998.

Defrise, M, Noo, F, and Kudo, H, (2001) A combination of rebinning and exact reconstruction algorithms for helical cone-beam scanning, *The sixth int. meeting on fully three-dimensinal image reconstruction in radiology and nuclear medicine,* Asilomar, Pacific Grove, CA, 30 Oct. – 2 Nov. pp 98-101

Grangeat, P. (1987), Analyse d'un systeme d'imagerie 3D par reconstrucion a partir de radiographies X en geometrie conique, Ph. D. thesis, Ecole Nationale Superieure des Telecommunications

Heuscher, D. J. (1999), Helical cone beam scans using oblique 2D surface reconstructions*,* 3D-1999, *The fifth int. meeting on fully three-dimensional image reconstruction in radiology and medicine*, Egmond Aan Zee, The Netherlands, June 23-26, pp 204-207

Hu, J, Johnson, R, and Dawson, C. (2001), Practical helical cone beam algorithm for the long object problem, *The sixth int. meeting on fully three-dimensinal image reconstruction in radiology and nuclear medicine,* Asilomar, Pacific Grove, CA, 30 Oct. – 2 Nov. pp 11 -14

Katsevich, A. (2001) Exact FBP-type inversion algorithm for spiral CT, *3D-2001, The sixth int. meeting on fully three-dimensinal image reconstruction in radiology and nuclear medicine,* Asilomar, Pacific Grove, CA, 30 Oct. – 2 Nov. pp 3-6

Kudo, H, Noo, F, and Defrise, M. (2001), Simple quasi-exact filtered backprojection algorithms for long-object problem in helical cone-beam tomography, *3D-2001, The sixth int. meeting on fully three-dimensional image reconstruction in radiology and nuclear medicine,* Asilomar, Pacific Grove, CA, Oct.30- Nov.2, pp 7 -10

Larson G. L., Ruth C. C., and Crawford C. R. (1998), Nutating slice CT image reconstruction*,* Patent Application WO 98/44847

Noo, F., Defrise, M., and Clackdoyle, R., (1998) Single-slice rebinning method for helical cone-beam CT, *Physics in Medicine and Biology*, **44** 561-570

Orlov, S.S. (1975), Theory of three-dimensional reconstruction – Conditions for a complete set of projections. *Sov.Phys. Crystallogr*. **20**, 312-314

Proksa, R, Köhler, T., Grass, M., Timmer, J. (2000), The n-PI-method for helical cone-beam CT. *Trans. on Medical Imaging*, **19**, 848-863

Sourbelle, K, Kudo, H, Lauritsch, G, Tam, K.C, Defrise, M, and Noo, F, 2001, Performance evaluation of exact cone-beam algorithms for the long-object problem in spiral computed tomography, *3D-2001, The sixth int. meeting on fully three-dimensional image reconstruction in radiology and nuclear medicine,* Asilomar, Pacific Grove, CA, 30 Oct. – 2 Nov., pp 153-156

Strierhofer, K., Flohr, T., Bruder, H., Segmented multiple plane reconstruction – A novel approximate reconstruction scheme for multislice spiral CT, *3D-2001, The sixth int. meeting on fully three-dimensional image reconstruction in radiology and nuclear medicine,* Asilomar, Pacific Grove, CA, 30 Oct. - 2 Nov., pp 95-97

Tam, K.C., (1995), Three-dimensional computerized tomography scanning method and system for large objects with small area detectors, US Patent 5,390,112.

Turbell, H, and Danielsson, P.-E. (2000), Helical Cone-beam Tomography, *Int. Journal of Imaging Systems and Technology,* **11,** 91-100

Turbell, H. (2001), Cone-beam reconstruction using filtered back-projection, Linköping Studies in Science and Techn

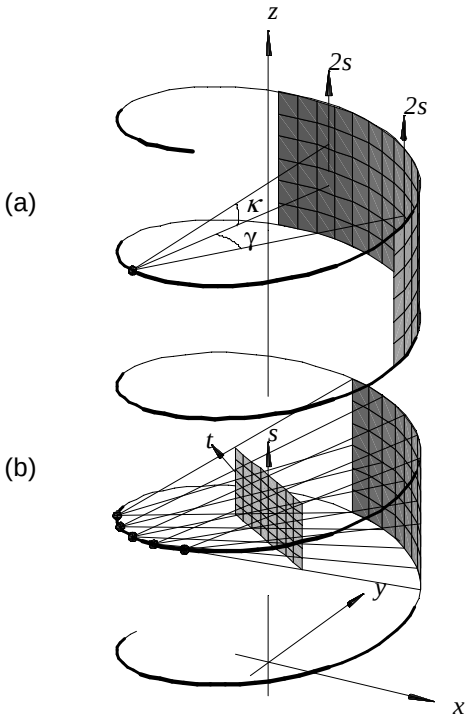

Figure 1. a) The TAM-window mapped onto the helix b) Rebinned PI-method geometry. Note the rectangular shape of the planar virtual detector

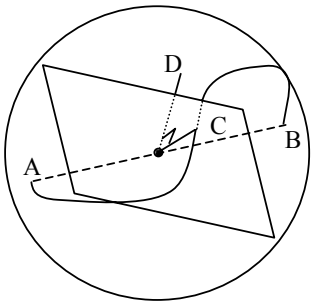

Figure 2. The local Fourier domain of a small volume element is completely swept out by source movements from A to B

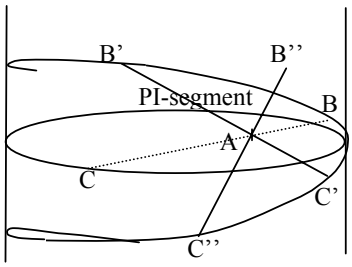

Figure 3. Each object point is on one and only one PI-line

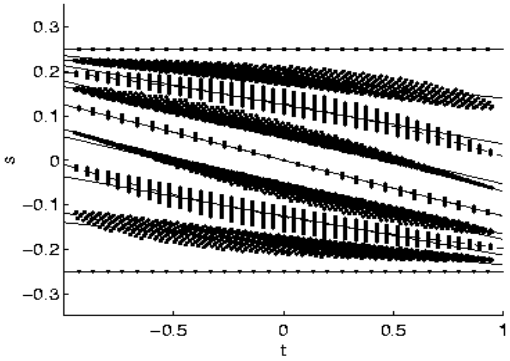

Figure 4. Projections of one PI-surface in nine consecutive phases of rotation

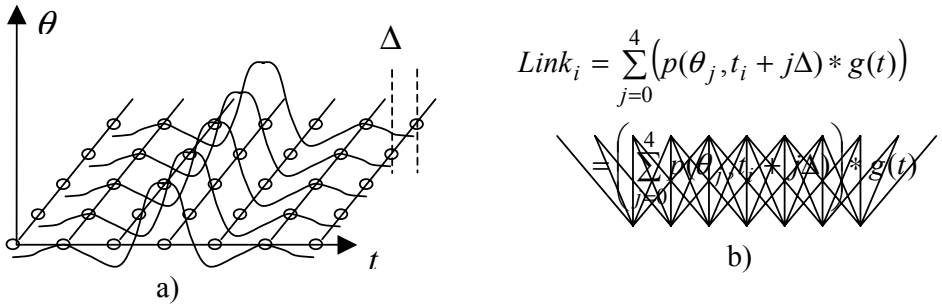

Figure 5. Ramp-filtering followed by back-projection over five projection angles $\theta_j = \theta_0 + \Delta\theta$ equals back-projection over the same projection angles followed by ramp-filtering

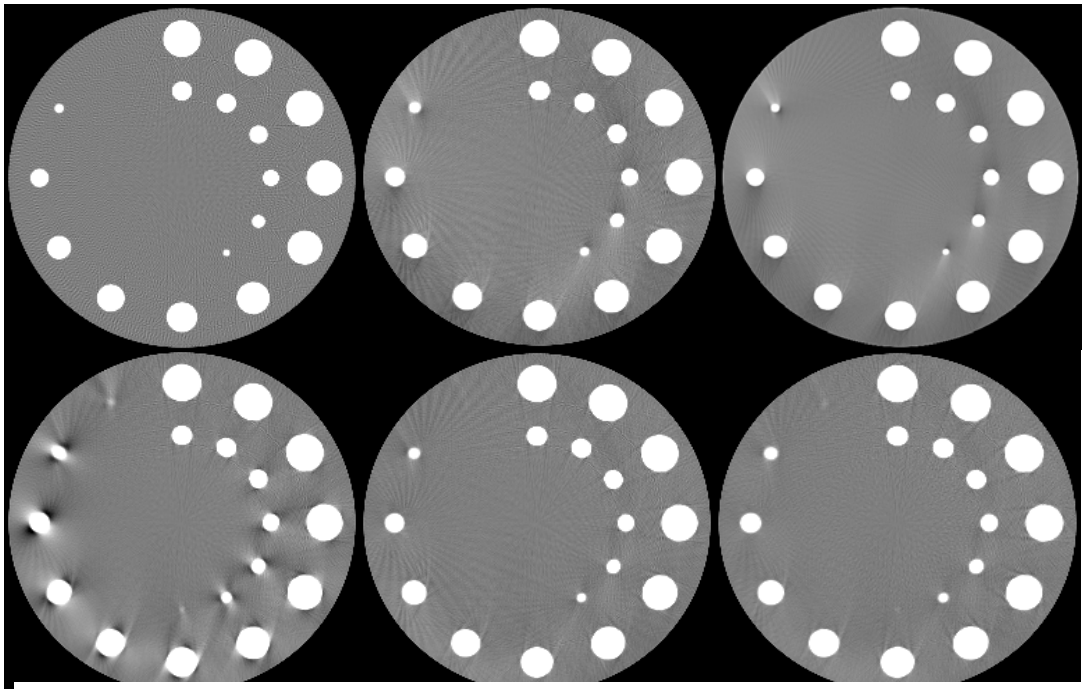

Figure 6. Experiment 1. Clockwise from upper left: 2D filtered back-projection, PI-ORIGINAL, PI-ORIGINAL with full resolution (Exp. 0), PI-FAST, PI-SLANT, PI-2D. Gray-level interval $\pm 50\,HU$

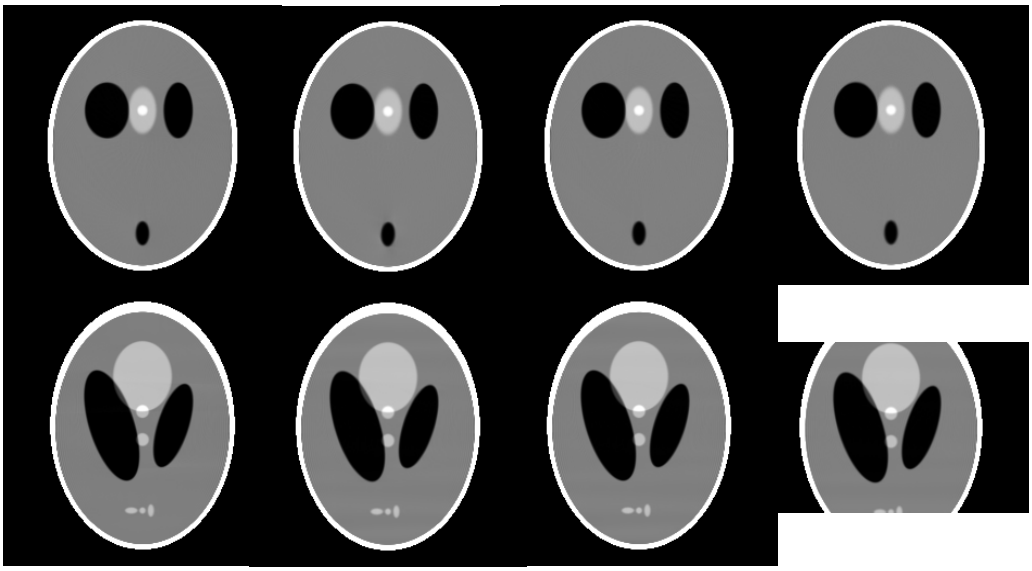

Fig. 7. Exp. 1. PI-ORIGINAL, PI-2D, PI-SLANT, PI-FAST. Upper row: xy-slice. Lower row: xz-slice. Far right: No artefacts for truncated long objects (holds for all PI-methods). Grey-level interval: $\pm 20\,HU$

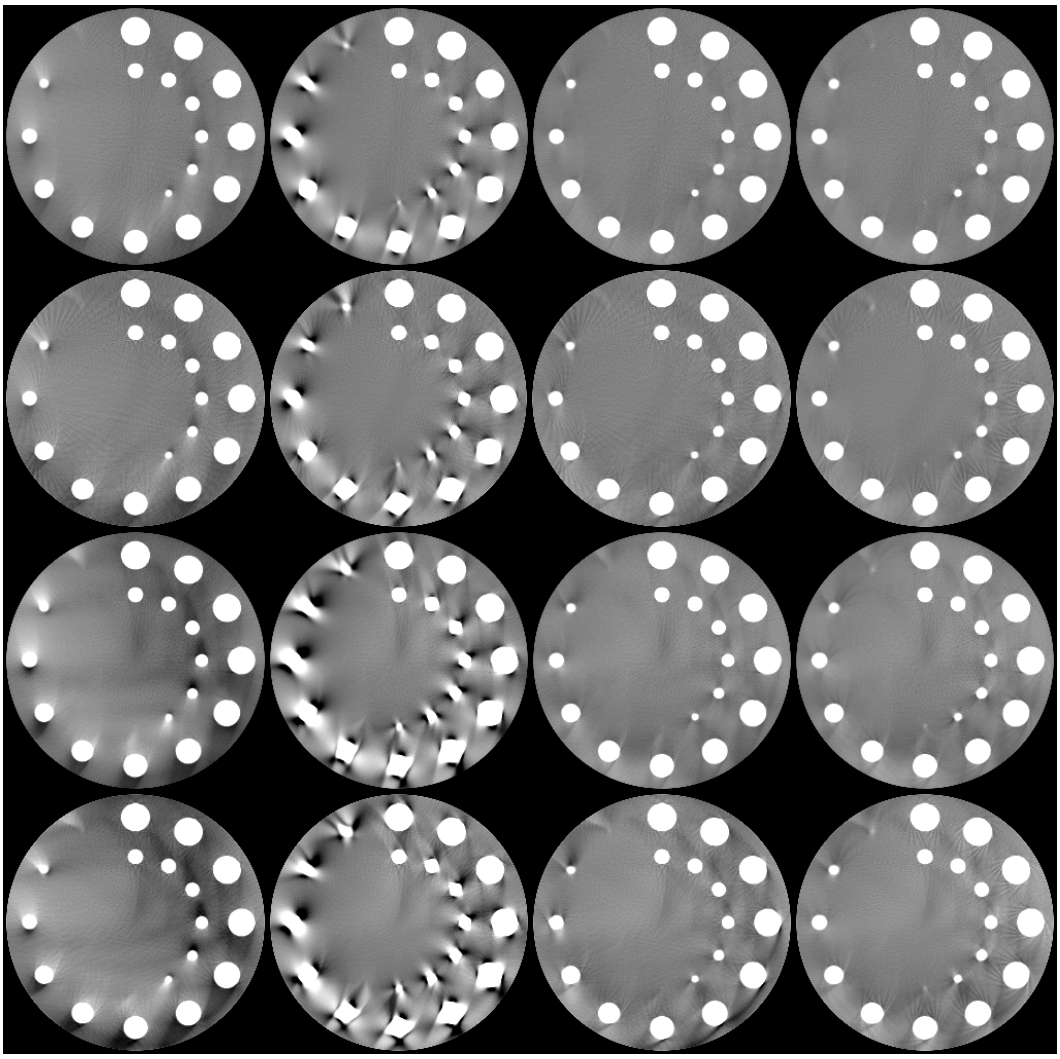

Fig. 8. From top : $(\gamma = 15^0, \kappa = 3.5^0)$, $(\gamma = 30^0, \kappa = 3.5^0)$, $(\gamma = 15^0, \kappa = 7^0)$, $(\gamma = 30^0, \kappa = 7^0)$
From left : ORIGINAL, 2D, SLANT, FAST. Grey-level interval: $\pm 50\,HU$